Tracking the rotation of single CdS nanorods during photocatalysis with surface plasmon resonance microscopy

Yingyan Jiang[a], Hua Su[a], Wei Wei[a], Yongjie Wang[a], Hong-Yuan Chen[a], and Wei Wang[a,1]

[a]State Key Laboratory of Analytical Chemistry for Life Science, School of Chemistry and Chemical Engineering, Nanjing University, 210023 Nanjing, China

While rotational dynamics of anisotropic nanoobjects has often been limited in plasmonic and fluorescent nanomaterials, here we demonstrate the capability of a surface plasmon resonance microscopy (SPRM) to determine the orientation of all kinds of anisotropic nanomaterials. By taking CdS nanorods as an example, it was found that two-dimensional Fourier transform of the asymmetrical wave-like SPRM image resulted in a peak in its angular spectrum in *k* space. Consistency between the peak angle and the geometrical orientation of the nanorod was validated by both in situ scanning electron microscope characterizations and theoretical calculations. Real-time monitoring of the rotational dynamics of single CdS nanorods further revealed the accelerated rotation under appropriate reaction conditions for photocatalyzed hydrogen generation. The driving force was attributed to the asymmetric production of hydrogen molecules as a result of inhomogeneous distribution of reactive sites within the nanorod. The present work not only builds the experimental and theoretical connections between the orientation of anisotropic nanomaterials and its SPRM images; the general suitability of SPRM also sheds light on broad types of nonfluorescent and nonplasmonic anisotropic nanoobjects from semiconductors to bacteria and viruses.

rotational dynamics | semiconductor photocatalysis | surface plasmon resonance microscopy | angular spectrum | nanomotor

Rotational motion of nanoobjects is an important feature that reveals and regulates their behaviors and functions, with implications in diverse fields ranging from biomechanics (1–6), nanomotors (7–10), enzymatic catalysis (11–13) to rheology, and fluid mechanics (14, 15). Tracking the dynamic orientation and rotation at single nanoobject level has proven powerful as it overcomes the averaging effect in ensemble measurements. Light microscopy that relies on the orientation-dependent optical property has been a major choice toward this goal (16–21), owing to its excellent compatibility with application environments and sufficient temporal and spatial resolutions. For example, differential interference contrast microscopy (1, 2, 5, 22–24), dark-field scattering microscopy (3, 4, 6, 25, 26) and anisotropic fluorescence microscopy (27, 28) have been widely utilized for studying plasmonic and fluorescent nanomaterials, respectively. However, many important anisotropic nanoobjects, such as semiconductors and biological particles (cell organelles, bacteria, and viruses), do not possess inherent fluorescent or plasmonic property and they can hardly be studied with the existing methods. An optical imaging technique that is suitable for all kinds of anisotropic nanoobjects, regardless of its inherent optical property, is thus highly desirable and it is yet to be demonstrated.

Surface plasmon resonance microscopy (SPRM) is a wide-field imaging technique that measures the dielectric constant of single nanoparticles based on its interaction with surface plasmon polaritons (SPPs) (29–33). Because dielectric constant is an inherent property of all kinds of materials, SPRM is capable of imaging broad types of nanomaterials including metal, semiconductor, polymer, and biological nanoparticles without the need of staining

or labeling (31, 32, 34–38). Near-field plasmonic enhancement, together with the linear dependence of SPRM signal on the nanoparticle volume, has ensured a good sensitivity to detect gold nanoparticles as small as 15 nm and silica nanoparticles as small as 50 nm. However, most SPRM studies so far have assumed the individual nanoobject as an isotropic sphere. Despite micrometer-scale anisotropic objects (nanowires and bacteria) being used in a few studies (39–41), dependence of the morphology and orientation of a nanoobject on its SPRM image remains completely unexplored. The clarification of such dependence should, in turn, offer a novel technique for studying the rotational dynamics of anisotropic nanomaterials with arbitrary chemical compositions.

Here we propose an angular spectrum approach to extract the orientation of single CdS nanorods from its SPRM image. The measured orientation was validated by the scanning electron microscopy (SEM) characterizations to the very same nanorod. We further propose a discrete convolution method (DCM) to calculate the SPRM image of nanoobjects with arbitrary morphology and orientation. The consistency between experimental results and theoretical calculations provides strong support on the validity of the angular spectrum approach. After demonstrating its capability for monitoring the orientation trajectories of multiple rotating CdS nanorods simultaneously, *in operando* rotational dynamics of single CdS nanorods was recorded under typical conditions for photocatalyzed hydrogen production. Surprisingly, the results uncovered an accelerated rotation of

Significance

Rotational dynamics of anisotropic nanomaterials reveals and regulates their behaviors and functions in diverse fields ranging from nanomotors, biomechanics, and enzymatic catalysis to microrheology. An optical imaging technique that is suitable for all kinds of anisotropic nanoobjects, regardless of its inherent optical property, is thus highly desirable and it is yet to be demonstrated. In the present work, by taking a nonfluorescent and nonplasmonic CdS nanorod as an example, we demonstrate the capability of a recently developed surface plasmon resonance microscopy for determining the orientation of single anisotropic nanomaterials with arbitrary chemical composition and morphology.

single CdS nanorods during photocatalysis, which was strong enough to trigger the rotation of a previously fixed nanocatalyst.

Results and Discussion

The principle, apparatus, and features of SPRM to visualize single nanoparticles have been described in detail in the literature (31, 32, 34–38). Briefly, a scattering wave is generated when propagating SPPs encounters a nanoparticle that is placed at the metal–dielectric interface. Interactions between the scattering wave and the SPPs alter the local reflectivity. Both theoretical (42) and experimental (43) studies have shown that an individual nanoobject appears as a wave-like pattern with parabolic tails (Fig. 1A), which describes the point-spread function (PSF) of SPRM. The orientation of the tail (upward) is consistent with the propagation direction of SPPs. While existing studies often focused on the dependence of SPRM signal on the nanoparticle size (31) and chemical composition (36) (dielectric constant), here we demonstrate the capability of SPRM to differentiate anisotropic from isotropic nanoparticles. As shown in Fig. 1A, when a spherical polystyrene nanoparticle is interacting with SPPs, a symmetrical wave-like pattern is always observed. However, when a nonspherical CdS nanorod takes a nonperpendicular orientation to the SPPs, the wave-like pattern becomes clearly asymmetric (Fig. 1B). These results suggest an opportunity to determine the nanorod orientation by analyzing the corresponding SPRM image.

It has been shown that two adjacent rings can be obtained in k space by applying a two-dimensional Fourier transform to the wave-like pattern (31). Fitting the rings with a circle equation further allowed for quantifying essential physical and geometric parameters to understand the interactions between nanoparticle and SPPs (43). In the present work, we made one critical step to extract an angular spectrum of the SPRM pattern in k space, from which the orientation of single CdS nanorods was determined. For example, in situ SEM image and the corresponding SPRM image of a 2-μm-long CdS nanorod are displayed in Fig. 2 A and B, respectively. They revealed an intersection angle of 118° to the propagation direction of SPPs (upward). In contrast to the symmetric rings for symmetric wave-like patterns (31, 43) (*SI Appendix*, Fig. S1), the same Fourier
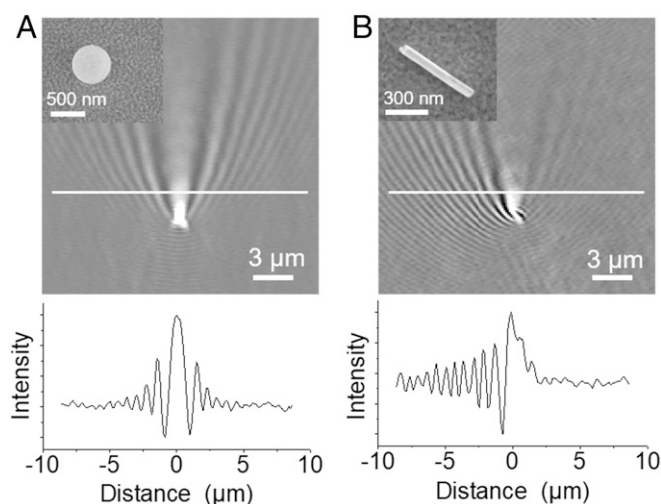

Fig. 2. (A) In situ SEM image of a 2-μm-long CdS NR shows an intersection angle of 118° between NR and propagation direction of SPPs. Both experimental SPRM pattern (B) and the corresponding k-space image (C) exhibit asymmetric features. A bright spot in the k-space ring has an angle of circumference close to 118°. (D) The experimental (black curve) and theoretical (red curve) angular spectra of the particular CdS NR shown in A are in good agreement with each other. The theoretical angular spectrum is extracted from the theoretical SPRM pattern (E) and the corresponding k-space image (F) according to DCM calculation.

transform to the asymmetric SPRM pattern (Fig. 2B) led to significantly asymmetric rings in k space (Fig. 2C). To extract the orientation information out of the ring, an angular spectrum analysis was conducted following the procedure below. The k-space image was fitted by a ring function (*SI Appendix*, Fig. S1) (43), which is illustrated by the red circle shown in Fig. 2C. The angular spectrum was subsequently defined as the local intensity along the circle as a function of the angle of circumference from 0 to 180°. As shown in Fig. 2D (black curve), the angular spectrum of the particular CdS nanorod reveals a clear peak at the angle of 118°, which perfectly matches the SEM characterizations (Fig. 2A). The uncertainty was mostly from the selection of region of interest (ROI). When choosing five different ROIs for the same nanorod in a series of SPRM images, we achieved a measurement uncertainty of ±4° (*SI Appendix*, Fig. S9).

We further proposed a DCM method to calculate the wave-like SPRM pattern of nanoobjects with arbitrary geometry (morphology and orientation), from which the theoretical angular spectrum can be obtained. DCM is based on the superposition principle of linear optical imaging systems. Briefly, the SPRM pattern of an object can be described as the convolution of its true geometry with the PSF. Since the PSF can be numerically calculated from electromagnetic theory (42), one is able to calculate the SPRM pattern of any object with given geometry (*SI Appendix*, Fig. S2). Taking the CdS nanorod shown in Fig. 2A as an example, the rod geometry (2-μm length and 60-nm width) was discretized to form a row of 33 horizontal pixels. Each pixel represented a cube of 60 nm. The 118° orientation of CdS nanorod was achieved by altering the propagation direction of SPPs, a parameter in the electromagnetic equation of PSF. DCM subsequently calculated the convolution of geometry matrix and PSF matrix, resulting in a theoretical SPRM pattern as shown in Fig. 2E. The calculated wave-like pattern was nicely consistent with the experimental results (Fig. 2B). For example, a locally enhanced interference pattern can be identified in both figures as indicated by white arrows. Furthermore, two-dimensional Fourier transform to Fig. 2E results in an asymmetric ring in k space as shown in Fig. 2F, of which the angular spectrum (red curve in Fig. 2D) is in excellent agreement with the experimental results (black curve in Fig. 2D). Both spectra clearly identified the peak at 118°, together with a series of minor periodic fluctuations. The consistency between experimental and theoretical results indicated that angular spectrum analysis was able to quantitatively determine the nanorod orientation from the

Fig. 1. Representative SPRM images of a spherical polystyrene NP (A) and a nonspherical CdS NR (B), respectively. (*Insets*) Corresponding SEM images of the very same nanoobjects with their actual orientations to the propagation direction of SPPs (upward). (*Bottom*) Intensity curves along the white lines are displayed, indicating the symmetric (A) and asymmetric (B) features in SPRM patterns.
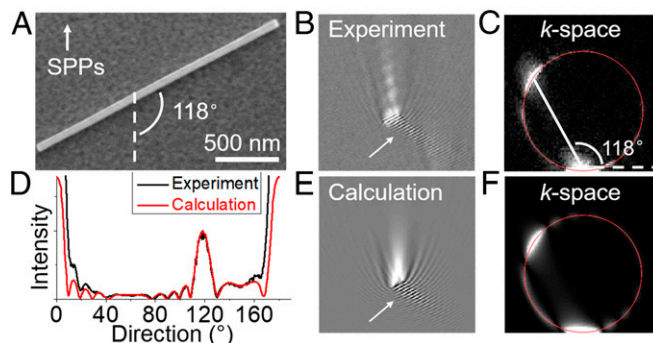
asymmetric SPRM pattern. Note that when the nanorod has a nonzero angle of elevation, DCM analysis is still able to report its orientation in the projection plane (*SI Appendix*, Fig. S8).

When the size of the nanorod was sufficiently large (longer than 1 μm, for instance), the nanorod orientation could be directly obtained from the characteristic peak in the angular spectrum (Fig. 2D). However, the signal-to-noise ratio of the angular spectrum became worse for nanorods with smaller size (*SI Appendix*, Fig. S3). When the length of the nanorod was shorter than 500 nm, it could be difficult to precisely determine the orientation from the angular spectrum itself. For example, the k-space ring and the corresponding angular spectrum of a short CdS nanorod are displayed in Fig. 3 A and B (black curve), respectively. In situ SEM reveals that the orientation angle is around 115° and the nanorod length is 415 nm (Fig. 3C). Theoretical angular spectrum of a 115° nanorod was also calculated by using the above DCM method and it is shown in Fig. 3C (red curve). Although the experimental and simulation results were consistent with each other, it was difficult to satisfactorily determine the orientation from the experimental value due to the noisy background.

Inspired by the recent applications of pattern recognition and machine learning in optical image processing (44), we developed a cross-correlation method to improve the accuracy when the angular spectrum itself was too noisy. This method was achieved by calculating the cross-correlation coefficient of the experimental angular spectrum with a series of reference spectra that were calculated under all possible orientations from 0 to 180° (*SI Appendix*, Fig. S4). The cross-correlation coefficient between the measured angular spectrum (black curve in Fig. 3B) and each of the reference spectra was subsequently calculated to generate a correlation curve shown in Fig. 3D (see *SI Appendix*, Fig. S5 for details). The maximal cross-correlation coefficient is detected at 115°, which is in agreement with the orientation angle. The correlation curve (Fig. 3D) took full advantage of all of the spectral features, and thus significantly improved the accuracy for determining the orientation angle.

We subsequently examined the capability of the above methods for determining and monitoring the rotational dynamics of three freely rotating CdS nanorods simultaneously. It was found that the interaction between as-prepared CdS nanorods and a gold-coated coverslip was highly dependent on the ionic strength

Fig. 4. (A) Representative rotational dynamics of a single CdS NR during the entire 15 min. (B) The distribution of CdS NR orientations during the rotation period (2–13 min).

of solution. When dilute CdS dispersion was added to a chamber containing pure water, most of the CdS nanorods were found to attach to the gold substrate with only one end. This end served as an anchor point to hold the nanorod close to the substrate, leaving the other end freely rotating in the water. Increasing the ionic strength was found to inhibit the rotation by laying down the nanorod onto gold film, suggesting that the electrostatic repulsion force between CdS nanorods and gold substrate was responsible for the translational and rotational behaviors in pure water. Time-lapsed SPRM images containing three rotating CdS nanorods were recorded and analyzed in a particle-by-particle and frame-by-frame manner. Angular spectrum of a nanorod was obtained by choosing the corresponding ROI in the SPRM image, conducting a two-dimensional Fourier transform, fitting the ring in k space, and calculating the cross-correlation curve to determine the orientation, sequentially. It was found that rotational dynamics among adjacent nanorods was highly stochastic and unsynchronized (*SI Appendix*, Fig. S6). Note that the translational dynamics was revealed from real-space SPRM images instead of k-space images. The location of the nanorod was determined by the cross-point in the wave-like SPRM pattern.

CdS nanorods are one kind of popular photocatalysts that can catalyze the generation of hydrogen molecules in the presence of hole scavengers and blue light. Note that the photocatalytic activity of as-prepared bulk CdS nanorods was validated by using a conventional reactor coupled with gas chromatography (*SI Appendix*, Fig. S7). While the accelerated motion and rotation has been a well-known phenomenon in enzymatic catalysis (12, 45), an interesting question here is how photocatalysis affects the rotational dynamics of single CdS nanorods under reaction conditions. In a typical experiment, before the irradiation of blue light, CdS nanorods did not exhibit any rotational activity due to the high ionic strength (10 mM Na_2S and 10 mM Na_2SO_3). After recording a baseline of 2 min, blue light (λ < 500 nm) began to illuminate the solution for 5 min to trigger the photocatalytic production of hydrogen. The blue light was turned off afterward and the SPRM images were recorded for another 8 min. Representative rotational dynamics of a single CdS nanorod during the entire 15 min is shown in Fig. 4A. Analysis of the occurrence probability of each orientation uncovers multiple preferable orientations of the nanorod (Fig. 4B). Different nanorods showed different preferred orientations. Such preferred orientations could be eliminated if the nanorod was freely rotating for a relatively longer period (*SI Appendix*, Fig. S13). A movie showing the dynamic rotation behaviors is also provided in *SI Appendix* (Movie S1). At the moment of light irradiation, a sudden change by 10° in the nanorod orientation was detected, likely due to the thermal-induced mechanical disturbance from the surrounding medium. This temperature change occurred and immediately reached a thermal equilibrium within 1 s.

The most interesting phenomenon was that, after a certain period of waiting time (30 s in this particular case), the nanorod was released from surface trapping and underwent rotational

Fig. 3. The k-space ring (A), the corresponding angular spectrum (B), and in situ SEM (C) of a 415-nm-long CdS NR. (D) The largest cross-correlation coefficient between experimental and theoretical spectra is obtained at 115°.

movements. Because the thermal equilibrium has been achieved, we attributed the accelerated rotation and translation to be the asymmetric production of hydrogen molecules as a result of inhomogeneous distribution of reactive sites within the nanorod. The release of hydrogen molecules induced a force onto the nanorod and led to the nanorod rotation when it overcame the interaction force between nanorod and substrate. Asymmetric release of product molecules has been proposed to understand the accelerated rotation of enzyme molecules (12, 45–48). The present work reports such effect for much bigger semiconductor nanomaterials that were previously fixed on the substrate. In a recent study, nanosized vapor steam bubbles were found to boost the rotation of a dimerized gold nanoparticle upon laser heating under liquid-cell transmission electron microscopy (49). The presence of a vapor steam nanobubble was excluded here because of the neglectable heating effect. We also excluded the existence of nanosized H_2 bubbles because of the following reasons. In our previous work (35), we have demonstrated that the SPRM technique is sufficiently sensitive to detect single H_2 nanobubbles as small as 40 nm. However, we did not detect the appearance of H_2 nanobubbles in the present study. More importantly, existing studies (35, 50, 51) indicated that an induction time of tens of minutes was necessary to saturate the local medium with H_2 molecules before the appearance of nanobubbles. In the present study, accelerated rotation was observed almost immediately after the light illumination. It was too fast to locally saturate the medium, an essential prerequisite for bubble nucleation. Therefore, the asymmetric release of hydrogen molecules was believed to be the reason for the accelerated rotation of CdS nanorods during photocatalysis.

The rotation directions of single CdS nanorods were randomly switching between clockwise and counterclockwise directions (*SI Appendix*, Fig. S12), because the production of H_2 molecules was temporally stochastic and spatially heterogeneous at single-nanorod level. Existing studies have shown that dynamic restructuring of surface atoms (52) and surface ligands (53) dramatically regulated the catalytic activity at single-nanoparticle level. Our recent study also indicated that H_2 molecules were stochastically generated at a portion of the reactive sites in single CdS nanoparticles (35). Therefore, it was reasonable to believe that, for single CdS nanorods, H_2 molecules did not constantly generate at the same subnanoparticle location. Instead, it was such temporal dynamics and spatial heterogeneity of producing H_2 molecules that were responsible for the random rotation direction.

The withdrawal of light irradiation did not stop the rotation of the nanorod immediately. Only after 6 min, the nanorod suddenly laid on the substrate again and remained still thereafter. Note that this postreaction time was rather random from particle to particle. Some nanoparticles kept rotating for a very long time until they ran away from the field of view. These results indicated that the rotational dynamics of single CdS nanorods was regulated by both thermodynamic motions and photocatalyzed H_2 production. First, it was frequently observed that some previously fixed CdS nanorods began to rotate after triggering the photochemical reactions (Fig. 4). Second, for those previously rotating CdS nanorods, quantitative analysis revealed accelerated rotation angular speed in the presence of light. The rotation angular speed was evaluated by both mean-square angular displacement (MSAD) method (54) and autocorrelation analysis (8). As shown in *SI Appendix*, Fig. S10, the presence of light was found to increase the MSAD slope and to decrease the characteristic time, both indicating the accelerated rotation speed as a result of photochemical reactions. Third, increasing the laser power was also found to increase the MSAD slope (*SI Appendix*, Fig. S11). These results demonstrated that, while thermodynamic motions inevitably were involved in the rotational dynamics, we

was still able to study the photocatalytic reactions of single CdS nanorods from its rotational dynamics.

Conclusion

In conclusion, we proposed an SPRM-based angular spectrum approach to determine the orientation of single CdS nanorods, which was validated by both experimental (SEM characterizations) and theoretical (DCM calculations) results. Temporal resolution and wide-field feature of SPRM allowed for simultaneously monitoring the trajectory of each individual to investigate its rotational dynamics under freestanding and photocatalysis conditions, respectively. The present study represents both scientific and technological advances. From the technical point of view, it is an attempt to resolve the orientation of anisotropic nanomaterials from its asymmetric wave-like patterns in SPRM. The introduction of DCM approach also provides a capability for calculating the SPRM patterns of nanomaterials with arbitrary geometry. The excellent agreement between experimental and simulation results, together with the in situ SEM characterizations, strongly validates the applicability of the present methods. From the scientific aspect, rotational dynamics is a means for evaluating the photocatalytic activity at single-nanocatalyst level. Existing single-nanoparticle catalysis studies often focused on nanocatalysts that were firmly immobilized on the substrate. A rotating nanocatalyst is certainly a better mimic to the real scenario, offering a perspective to the field of single-nanoparticle catalysis. In addition, although both the accelerated rotation of enzyme molecules during enzymatic reaction and the gas bubble propelled rotation of micromotors are well known, much less attention has been paid to their nanocatalyst counterpart despite the great value of nanocatalysis. The accelerated rotation of single nanocatalysts reported in the present work sheds light on the gap between enzymatic catalysis and micromotors. Furthermore, while existing single-nanoparticle rotational studies are often limited in fluorescent and plasmonic nanomaterials, the applicability of SPRM for all kinds of anisotropic nanoobjects opens significant possibility on broad areas involving optically inert nanoobjects, such as the transportation of mitochondrion and rod-like virus and bacterium (*SI Appendix*, Fig. S14), and the guided orientation of magnetic nanomaterials under magnetic field.

Materials and Methods

Materials. Polystyrene (PS) nanoparticles (NPs) were purchased from Aladdin as aqueous solution and used without further purification. Appropriate amount of PS NP solution was diluted with deionized water (DIW, 18.2-MΩ·cm resistivity). The size of PS NPs was characterized by SEM (JSM-7800F).

The CdS nanorods (NRs) were synthesized through a simple solvent thermal method according to the previous procedures (35, 55). Typically, 3 mmol of Cd(NO$_3$)$_2$·4H$_2$O and 9 mmol of thiourea were successively dissolved in anhydrous ethylenediamine, and then added into an autoclave with a Teflon inner which was filled to 60% of its capacity (25 mL) and maintained at 160 °C in a hot oven for about 22 h. The formed yellow precipitate was carefully collected by centrifugation and washed with plenty of distilled water and ethanol. After being dried under vacuum at 60 °C for 12 h, the as-obtained CdS NRs were characterized by SEM (JSM-7800F) to determine the morphology and size of NRs.

SPRM Setups for Single-NR Experiments. The experiment of SPRM imaging was performed on an inverted microscope (Nikon Ti-E). A supercontinous white laser (EXR-15; NKT Photonics), which was equipped with an acoustooptical tunable filter (SuperK SELECT VIS-NIR), was used as the light source. The monochromatic beam was collimated and focused at the back-focal plane of an objective lens with high numerical aperture (Nikon Apo TIRF 60× N.A. 1.49 oil immersion objective), resulting in a parallel illumination toward a gold-coated coverslip (47 nm Au with 2-nm Cr adhesion layer) with a certain incident angle. A polarizer was set in the optical path to generate p-polarized light to excite the surface plasmon wave. The SPRM images were recorded by a CCD camera (Pike F-032B; Allied Vision Technologies).

Correlated SPRM and SEM. The gold-coated coverslips were rinsed with DIW and ethanol, and blown dry under nitrogen before use. The gold-coated coverslips were assembled with a polydimethylsiloxane (PDMS) chamber (FlexiPERM micro 12). To immobilize CdS NRs on the gold-coated coverslip, 100 μL of CdS dispersions (0.01 μg·mL^{-1}) was added into the chamber and dried under vacuum at 50 °C overnight. An incident light with wavelength of 680 nm was utilized at a gold–air interface to obtain SPRM images of several CdS NRs and their corresponding SEM images were also recorded, to prove the feasibility of SPRM to identify the actual orientation of NRs.

Rotation of Single CdS NRs in Photocatalysis. The CdS NRs were dispersed in 0.1 M Na$_2$S (10 μg·mL^{-1}) firstly and the 5 μL diluted dispersion was added to the chamber containing a solution of 10 mM Na$_2$S and 10 mM Na$_2$SO$_3$. To ensure the integrity of the rings in k space, a 720-nm beam was utilized to totally reflect at the gold–solution interface with a resonance angle at about 68° to monitor the CdS NRs. A white-light source (X-cite 110LED, 110 W; Excelitas Technologies Corp.) coupled with a low-pass filter ($\lambda < 500$ nm) through a condenser (N.A. = 0.52) was focused to the coverslip to trigger the photocatalytic hydrogen generation reactions of the CdS NRs, which induced the rotation of the NRs.

1. Wang G, Sun W, Luo Y, Fang N (2010) Resolving rotational motions of nano-objects in engineered environments and live cells with gold nanorods and differential interference contrast microscopy. *J Am Chem Soc* 132:16417–16422.
2. Gu Y, et al. (2012) Rotational dynamics of cargos at pauses during axonal transport. *Nat Commun* 3:1030.
3. Xiao L, Wei L, Liu C, He Y, Yeung ES (2012) Unsynchronized translational and rotational diffusion of nanocargo on a living cell membrane. *Angew Chem Int Ed Engl* 51: 4181–4184.
4. Lebel P, Basu A, Oberstrass FC, Tretter EM, Bryant Z (2014) Gold rotor bead tracking for high-speed measurements of DNA twist, torque and extension. *Nat Methods* 11: 456–462.
5. Chen K, et al. (2017) Characteristic rotational behaviors of rod-shaped cargo revealed by automated five-dimensional single particle tracking. *Nat Commun* 8:887.
6. Kaplan L, Ierokomos A, Chowdary P, Bryant Z, Cui B (2018) Rotation of endosomes demonstrates coordination of molecular motors during axonal transport. *Sci Adv* 4: e1602170.
7. Jones PH, et al. (2009) Rotation detection in light-driven nanorotors. *ACS Nano* 3: 3077–3084.
8. Qin W, et al. (2017) Catalysis-driven self-thermophoresis of Janus plasmonic nanomotors. *Angew Chem Int Ed Engl* 56:515–518.
9. Shao L, Yang ZJ, Andrén D, Johansson P, Käll M (2015) Gold nanorod rotary motors driven by resonant light scattering. *ACS Nano* 9:12542–12551.
10. Shao L, Kall M (2018) Light-driven rotation of plasmonic nanomotors. *Adv Funct Mater* 28:1706272.
11. Uchihashi T, Iino R, Ando T, Noji H (2011) High-speed atomic force microscopy reveals rotary catalysis of rotorless F$_1$-ATPase. *Science* 333:755–758.
12. Riedel C, et al. (2015) The heat released during catalytic turnover enhances the diffusion of an enzyme. *Nature* 517:227–230.
13. Sun L, et al. (2017) Real-time imaging of single-molecule enzyme cascade using a DNA origami raft. *J Am Chem Soc* 139:17525–17532.
14. Rodríguez-Sevilla P, et al. (2016) Optical torques on upconverting particles for intracellular microrheometry. *Nano Lett* 16:8005–8014.
15. Li S-J, Qian H-J, Lu Z-Y (2018) Translational and rotational dynamics of an ultra-thin nanorod probe particle in linear polymer melts. *Phys Chem Chem Phys* 20: 20996–21007.
16. Gu Y, et al. (2013) Single particle orientation and rotational tracking (SPORT) in biophysical studies. *Nanoscale* 5:10753–10764.
17. Xiao L, Yeung ES (2014) Optical imaging of individual plasmonic nanoparticles in biological samples. *Annu Rev Anal Chem* (Palo Alto, CA) 7:89–111.
18. Peng Y, et al. (2015) Recent advances in optical imaging with anisotropic plasmonic nanoparticles. *Anal Chem* 87:200–215.
19. Anthony SM, Yu Y (2015) Tracking single particle rotation: Probing dynamics in four dimensions. *Anal Methods* 7:7020–7028.
20. Ha JW (2016) Recent advances in single particle rotational tracking of plasmonic anisotropic gold nanoparticles under far-field optical microscopy. *Appl Spectrosc Rev* 51:552–569.
21. Gao Y, Yu Y, Sanchez L, Yu Y (2017) Seeing the unseen: Imaging rotation in cells with designer anisotropic particles. *Micron* 101:123–131.
22. Gu Y, Sun W, Wang G, Fang N (2011) Single particle orientation and rotation tracking discloses distinctive rotational dynamics of drug delivery vectors on live cell membranes. *J Am Chem Soc* 133:5720–5723.
23. Xiao L, Ha JW, Wei L, Wang G, Fang N (2012) Determining the full three-dimensional orientation of single anisotropic nanoparticles by differential interference contrast microscopy. *Angew Chem Int Ed Engl* 51:7734–7738.
24. Lee IB, et al. (2018) Interferometric scattering microscopy with polarization-selective dual detection scheme: Capturing the orientational information of anisotropic nanometric objects. *ACS Photonics* 5:797–804.
25. Xiao L, Qiao Y, He Y, Yeung ES (2011) Imaging translational and rotational diffusion of single anisotropic nanoparticles with planar illumination microscopy. *J Am Chem Soc* 133:10638–10645.
26. Ha JW, Marchuk K, Fang N (2012) Focused orientation and position imaging (FOPI) of single anisotropic plasmonic nanoparticles by total internal reflection scattering microscopy. *Nano Lett* 12:4282–4288.
27. Tsyboulski DA, Bachilo SM, Kolomeisky AB, Weisman RB (2008) Translational and rotational dynamics of individual single-walled carbon nanotubes in aqueous suspension. *ACS Nano* 2:1770–1776.
28. Loumaigne M, Richard A, Laverdant J, Nutarelli D, Débarre A (2010) Ligand-induced anisotropy of the two-photon luminescence of spherical gold particles in solution unraveled at the single particle level. *Nano Lett* 10:2817–2824.
29. Huang B, Yu F, Zare RN (2007) Surface plasmon resonance imaging using a high numerical aperture microscope objective. *Anal Chem* 79:2979–2983.
30. Wang W (2018) Imaging the chemical activity of single nanoparticles with optical microscopy. *Chem Soc Rev* 47:2485–2508.
31. Halpern AR, Wood JB, Wang Y, Corn RM (2014) Single-nanoparticle near-infrared surface plasmon resonance microscopy for real-time measurements of DNA hybridization adsorption. *ACS Nano* 8:1022–1030.
32. Wang S, et al. (2010) Label-free imaging, detection, and mass measurement of single viruses by surface plasmon resonance. *Proc Natl Acad Sci USA* 107:16028–16032.
33. Nizamov S, Kasian O, Mirsky VM (2016) Individual detection and electrochemically assisted identification of adsorbed nanoparticles by using surface plasmon microscopy. *Angew Chem Int Ed Engl* 55:7247–7251.
34. Yang Y, et al. (2015) Label-free tracking of single organelle transportation in cells with nanometer precision using a plasmonic imaging technique. *Small* 11:2878–2884.
35. Fang Y, et al. (2017) Intermittent photocatalytic activity of single CdS nanoparticles. *Proc Natl Acad Sci USA* 114:10566–10571.
36. Jiang D, et al. (2017) Optical imaging of phase transition and Li-ion diffusion kinetics of single LiCoO(2) nanoparticles during electrochemical cycling. *J Am Chem Soc* 139: 186–192.
37. Cho K, Fasoli JB, Yoshimatsu K, Shea KJ, Corn RM (2015) Measuring melittin uptake into hydrogel nanoparticles with near-infrared single nanoparticle surface plasmon resonance microscopy. *Anal Chem* 87:4973–4979.
38. Maley AM, Lu GJ, Shapiro MG, Corn RM (2017) Characterizing single polymeric and protein nanoparticles with surface plasmon resonance imaging measurements. *ACS Nano* 11:7447–7456.
39. Yu H, Shan X, Wang S, Chen H, Tao N (2014) Plasmonic imaging and detection of single DNA molecules. *ACS Nano* 8:3427–3433.
40. Syal K, et al. (2016) Antimicrobial susceptibility test with plasmonic imaging and tracking of single bacterial motions on nanometer scale. *ACS Nano* 10:845–852.
41. Wang Y, Shan X, Wang H, Wang S, Tao N (2017) Plasmonic imaging of surface electrochemical reactions of single gold nanowires. *J Am Chem Soc* 139:1376–1379.
42. Yu H, Shan X, Wang S, Chen H, Tao N (2014) Molecular scale origin of surface plasmon resonance biosensors. *Anal Chem* 86:8992–8997.
43. Jiang Y, Wang W (2018) Point spread function of objective-based surface plasmon resonance microscopy. *Anal Chem* 90:9650–9656.
44. Zhong Y, Li C, Zhou H, Wang G (2018) Developing noise-resistant three-dimensional single particle tracking using deep neural networks. *Anal Chem* 90:10748–10757.
45. Kurzthaler C, et al. (2018) Probing the spatiotemporal dynamics of catalytic Janus particles with single-particle tracking and differential dynamic microscopy. *Phys Rev Lett* 121:078001.
46. Slochower DR, Gilson MK (2018) Motor-like properties of nonmotor enzymes. *Biophys J* 114:2174–2179.
47. Qin W, et al. (2017) Catalysis-driven self-thermophoresis of Janus plasmonic nanomotors. *Angew Chem Int Ed Engl* 56:515–518.
48. Golestanian R (2015) Enhanced diffusion of enzymes that catalyze exothermic reactions. *Phys Rev Lett* 115:108102.
49. Fu X, Chen B, Tang J, Hassan MT, Zewail AH (2017) Imaging rotational dynamics of nanoparticles in liquid by 4D electron microscopy. *Science* 355:494–498.
50. Su H, Fang Y, Chen F, Wang W (2018) Monitoring the dynamic photocatalytic activity of single CdS nanoparticles by lighting up H$_2$ nanobubbles with fluorescent dyes. *Chem Sci (Camb)* 9:1448–1453.
51. Li S, et al. (2017) Nanobubbles: An effective way to study gas-generating catalysis on a single nanoparticle. *J Am Chem Soc* 139:14277–14284.
52. Xu W, Kong JS, Yeh Y-TE, Chen P (2008) Single-molecule nanocatalysis reveals heterogeneous reaction pathways and catalytic dynamics. *Nat Mater* 7:992–996.
53. Zhang Y, et al. (2015) Superresolution fluorescence mapping of single-nanoparticle catalysts reveals spatiotemporal variations in surface reactivity. *Proc Natl Acad Sci USA* 112:8959–8964.
54. Ye Z, et al. (2019) Single-particle tracking discloses binding-mediated rocking diffusion of rod-shaped biological particles on lipid membranes. *Chem Sci* 10:1351–1359.
55. Jang JS, Joshi UA, Lee JS (2007) Solvothermal synthesis of CdS nanowires for photocatalytic hydrogen and electricity production. *J Phys Chem C* 111:13280–13287.